Revised version submitted to Journal of Synchrotron Radiation

High pressure and temperature spinning capillary cell for *in situ* synchrotron X-ray powder diffraction

Edmundo Fraga,[a,b] Armando Yáñez,[b] Jesus D. Zea-Garcia,[c] Angeles G. De la Torre,[c] Ana Cuesta,[c] Ricardo Valcárcel-Fernández,[a] Francesc Farré-París,[a] Marc Malfois,[a] Miguel A. G. Aranda[a,c*]

[a]ALBA Synchrotron, Carrer de la Lum, 2-26, 08290 Cerdanyola del Vallès, Barcelona, Spain. [b]Universidade da Coruña, Dpto. Departamento de Ingeniería Naval e Industrial, Campus de Esteiro s/n, 15403 Ferrol, A Coruña, Spain. [c]Departamento de Química Inorgánica, Universidad de Málaga, Campus Teatinos S/N, 29071 Málaga, Spain *Correspondence e-mail: migarcia@cells.es

In situ research of materials under moderate pressures, hundreds of bars, is essential in many scientific fields. These range from gas sorption to chemical and biological processes. One industrially-important discipline being the hydration of oil well cements. Existing capillary cells, in this pressure range, are static as they are easy to design and operate. This is convenient for the study of single phase materials however, powder diffraction quantitative analyses for multiphase systems cannot be performed accurately as good powder average cannot be attained. Here, we report the design, construction and commissioning of a cost-effective spinning capillary cell for *in situ* powder X-ray diffraction, currently up to 200 bars. The design addresses the importance of reducing the stress on the capillary by mechanically synchronize the applied rotation power and alignment on both sides of the capillary while allowing the displacement of the supports needed to accommodate different capillaries sizes and to insert the sample within the tube. This cell can be utilized for multiple purposes allowing the introduction of gas or liquid from both ends of the capillary. The commissioning is reported for the hydration of a commercial oil well cement at 150 bars and 150 ºC. The quality of the resulting powder diffraction data has allowed *in situ* Rietveld quantitative phase analyses for a hydrating cement containing seven crystalline phases.

Keywords: high-pressure equipment; oil well cement; cement hydration; Rietveld quantitative phase analysis

1. Introduction

Sample environments specifically designed for *in situ* powder synchrotron X-ray diffraction studies under high pressure and temperature are essential in many research fields. These scientific areas include gas sorption of many kinds, chemical and biological reactions, characterization of materials behaviour and they have been extensively discussed (Jupe & Wilkinson, 2006; Hansen *et al.*, 2015; Sakaki *et al.*, 2018). These capillary cells, which allow *in situ* studies in the hundreds of bars region, are static and allow to characterize the structural changes of a single phase under different gases (Hansen *et al.,* 2015; Sakaki *et al.,* 2018) or to follow the phase development in hydrating oil well cements (Jupe & Wilkinson, 2006).

However with static cells, powder diffraction quantitative studies for multiphase systems cannot be performed properly as good powder average cannot be attained. To ensure good particle averaging is essential for the study of several commercially relevant systems like oil well cement hydration. The relevance of spinning the samples in powder diffraction, and its implication for particle statistics, has been already discussed (Ida *et al.*, 2009).

For capillary cells, also known as microreactors, there is an intermediate possibility. It is common practice to increase the particle statistics, in the volume probed by the X-rays, by rocking the cell 5-10 degrees on its axis. It has been very recently reported a review on capillary cells containing key references dealing with rocking cells (van Beek & Pattison, 2018).

Synchrotron radiation is especially useful for the *in situ* characterization of processes because it is possible to select an X-ray beam of high energy (enables penetration) with very high flux (permits good signal-to-noise ratio). A review focused on the uses of synchrotron techniques for the study of building materials has been already published (Aranda, 2016). This paper is framed within our

research efforts to characterize *in situ* cement hydration by synchrotron techniques. Here, we report the development of spinning capillary cell which allows *in situ R*ietveld quantitative phase analyses of hydrating cements. Furthermore, this cell can be easily adapted for gas sorption studies by swapping the pressure transmitting agent from oil to the appropriate gas.

2. Materials and methods

2.1. Spinning capillary cell

2.1.1. General description. The cell is composed of a high pressure resistant capillary, where the sample is loaded, two side supports to connect the rotating capillary to the pressure measurement system and the pressure mean, a linear displacement system to be able to accommodate different capillary sizes and to access the interior of the capillary to change the sample, a transmission system which applies the rotation power to the capillary, a spring lock system to automatically lock the system before applying pressure and a heating system to reach the target temperature. The main components of this cell are sketched in Fig. 1. The 3D design is shown in supporting information as Fig. S1.

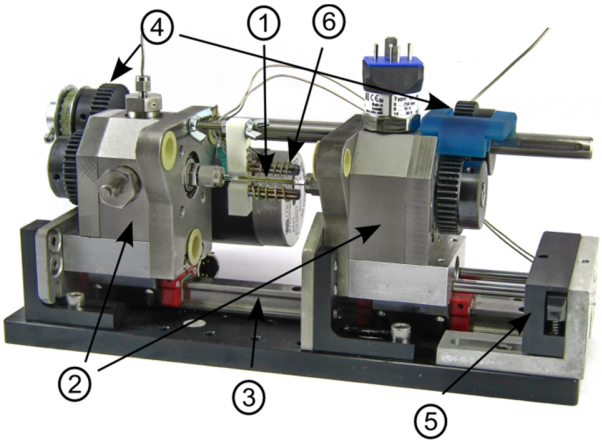

Figure 1.
Photograph of the built spinning cell with its main components described. Main components: 1. Sample holder (removable capillary). 2. Side supports. 3. Linear displacement system. 4. Transmission system. 5. Spring lock system. 6. Heating system.

2.1.2. Sample holder. For this commissioning study, the sample holders are 'single-crystal' sapphire capillaries supplied by Saint-Gobain crystals. These capillaries are grown along the *c*-axis direction, (0001) plane. The outer and inner diameters of the sapphire tubes are 3.18 mm and 1.75 mm, respectively. It is difficult to estimate the rupture stress defects for such a small single crystal as defects and micro fractures vary considerably and they are the main source of fracture. According to the manufacturer these capillaries can handle pressures up to around 550 bars with 2× factor of safety at room temperature. However as discussed by Azhdari *et al.*, (1998) different crystallographic planes have different surface energies being the planes $(1\bar{1}02)$ and $(11\bar{2}3)$, with low fracture surface energies, the ones that will support more sheer stresses under the torque needed to rotate. Other materials for capillaries (titanium or steel) can withstand higher pressures but it is necessary to use higher energy synchrotron radiation in order to penetrate these metal tubes.

The relation between the ultimate tensile strength of sapphire and the burst pressure for thin-walled capillaries has been studied (Jensen *et al.,* 2010). For sapphire capillaries of 1.09 mm outer diameter and 0.79 mm inner diameter, supplied by Saint-Gobain Crystals, the burst pressure was measured to be 900 bars. It was also stated that capillaries from other manufacturer, with lower quality, burst at a much lower pressure. A wider discussion on this topic has been recently reported by the same group (Hansen et al., 2015).

In any case, when using sapphire, it is essential to reduce the torque on the capillary. This was done avoiding any misalignment on both sides of the supporting axis, and synchronizing the torque applied on both sides leaving only a low amount of inertia torque that will be reduced with long (slow) accelerations.

2.1.3. Side supports. The capillary is supported in two shafts made from AISI310 stainless steel which is known to have good strength and good resistance to corrosion and oxidation at elevated temperatures and pressures. In one of its ends has a two-ferrule tube compression fitting size 1/8. The ferrules are made of a mixture of polyimide and graphite (Teide™ from Teknokroma), which were selected due to their capabilities to seal against sapphire with little force and so avoiding any extra stress on the capillary. Then, a hole in the centre of the axis reaches the middle to have access to the main pressure exchanger

chamber where the pressure mean, or the sample in case of continuous flow, enters into the axis. On the other end the axis has an adaptor to install a carbon steel spur gear (SS1-40C from KHK) with 40 teeth, module 1 and an inner diameter of 12 mm that will drive the spinning.

The axis is mounted in an asymmetric bearing cross-located design with two angular contact ball bearings in back-to-back configuration. The intention is to have a located axis that won't move under different pressures and have a big front bearing that can accommodate the rotation radial loads and axial loads from the pressure forces and channel then to the main support. This inner bearing, the closest to the sample, is a single row angular contact ball bearing (7200BEP from SKF); this kind of bearing can support normal axial loads at high speeds and channel the force to the main support. The main components of the side supports are depicted in Fig. 2.

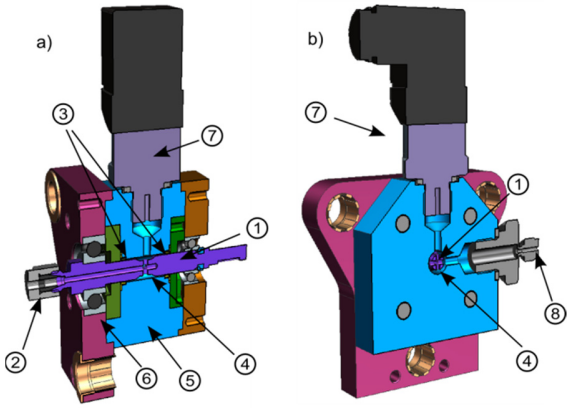

Figure 2
Cross sections of the side supports. a) Longitudinal view. b) Transversal view. 1. Main shaft. 2. Tube compression fitting system. 3. PTFE seals. 4. Exchanger chamber. 5. Support body. 6. Front bearing. 7. Pressure measurement. 8. Pressure inlet.

The support body is the exchanger part, it has two pressure entrances, one is used to insert the pressure into the exchanger chamber and the other one can be used to measure the pressure inside that chamber. The direct pressure measurement system (A-10 from WIKA) inside this exchanger chamber assures that the pressure is transmitted into the capillary as it is connected by four holes and an unlikely blockage in a hole would have negligible effects. The axis is sealed with two PTFE seals (FlexiSeal® with a FLO profile from PARKER), as they are suitable for both liquids and gases and the pressure range of application goes up to 200 bars and from -260 ºC to +315 ºC in temperature.

2.1.4. Linear displacement system. The two side supports are installed into two Schneeberger carriages that run into a linear ball guides monorail with the highest accuracy range from the manufacturer G0 that describes the vertical and horizontal deviations in parallelism in the carriages whilst moving over the guide rail. This, together with the restricted tolerances in dimensions and parallelism used to manufacture the support, results in a high degree of collinearity in both axes, one of the conditions to avoid stresses on the capillary and specially the very dangerous combinations of rotation and bending momentums that can lead to a fracture by fatigue.

2.1.5. Transmission system. The transmission consists of a 12 mm shaft driven by a stepper motor through a pulley transmission. This shaft is connected to the main axes by two carbon steel spur gears 40 tooth and module 1. The connection is made with a key system that prevents relative rotation and assures the same position of the gears to have a synchronize movement into both sides of the capillary, on top of that one of the two train gear can be displaced into the driving shaft while the key systems disable the rotation. This approach allows the cell to be quickly opened and closed to access the inside of the capillary for sample exchange while maintaining the tooth synchronization on both sides. The spinning is always made in the same direction to avoid backlash on the tooth contact. Here, it is used long accelerations times, around 10 seconds to reach a speed of 250 rpm, to minimize mechanical stress. The components of the transmission system are depicted in Fig. 3.

2.1.6. Spring lock system. The cell has an automatic spring lock system to be able to quickly change the sample and as a safety system to avoid the movement of the carriages in the rail. When the capillary size is adjusted, the movement of the carriages to open/close is automatically locked without any need of fixing by any other method.

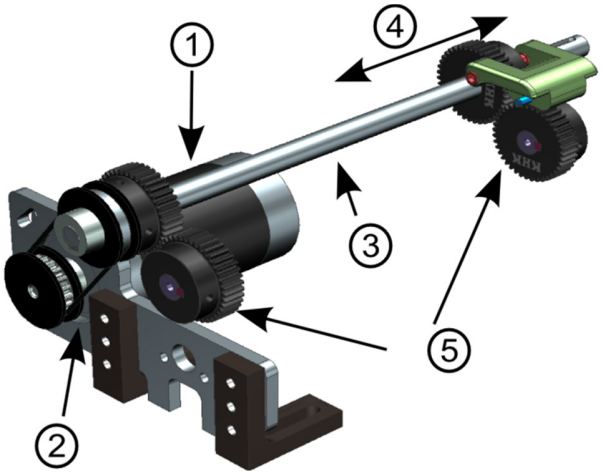

Figure 3

Transmission system. 1. 2-phase hybrid stepper motor with a holding torque 1.2Nm. 2. Metric timing pulleys system t5 pitch. 3. Main 12mm transmission shaft. 4. horizontal geared displacements. 5. Spur gears system module 1, 40 tooth and precision grade N8.

2.1.7. Pressure generator by oil. In this case, hydration of cements, static pressure was produced with equipment similar to that reported by Jupe & Wilkinson (2006). It contains a mineral light white oil pressure transmitting medium (Kaydol-type from Sigma-Aldrich). The pressure is generated by a manual pump generator by HiP with a range of 0 – 2000 bars. For safety reasons, the pressure generator assembly is equipped with a rupture disc for overpressure protection. In the existing configuration, the rupture disc is set at 200 bars. The system has a pressure transducer (HP-2 from WIKA) to have a pressure measurement in the generator with a range of 0 - 2500 bars together with a pressure gauge and it is connected to the cell using a 1/16 inches stainless steel capillary tube with an outside diameter of 1/16 inches. The components of the pressure generator are depicted in Fig. 4.

For gas sorption experiments, the pressure generator system should be exchanged by the gas pressure equipment. As the capillary is accessible through both sides, the implementation of the gas loading is straightforward, for non-hazardous gasses.

2.1.8. Heating system. The heating system consist on a resistive 1.2 mm Inconel-sheathed Thermocoax heating wire wrapped around a stainless steel 6 mm rod and mounted into a Macor® holding frame (Chupas *et al.,* 2008). The temperature inside the capillary is monitored with K-type thermocouple positioned into the Macor® frame and calibrated to compensate the offset between both positions. The resistance is powered by a power supply connected to a Eurotherm Nanodac® that records both the pressure and temperature and has a PID control.

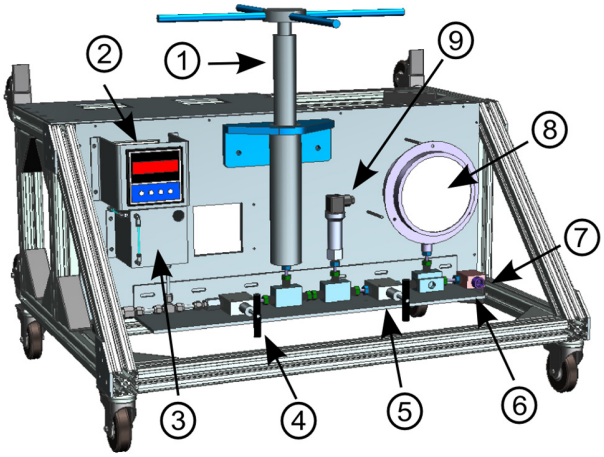

Figure 4

Pressure generator. 1. Manual Pressure Pump Generators. 2. Digital pressure display. 3. Oil tank at atmospheric pressure. 4. Inlet high pressure valve. 5. Outlet high pressure valve. 6. Rupture disc for overpressure protection. 7. Outlet to the cell. 8. Pressure gauge. 9. Pressure transducer.

To evaluate the possible impact of deformation due to the pressure forces and also to check the static stresses in the system, a finite element structural analysis (FEA) was carried out using the linear solver Siemens NX Nastran 11 (Sol101). Under a pressure of 20 MPa (200 bars), it was found a maximum equivalent tensile stress of 154.92 MPa bellows the yield strength limit of 200MPa for AISI 301. A horizontal nodal displacement under 6 microns that should not affect the alignment, and an irrelevant vertical displacement under 1 micron that would have a negligible effect on the misalignments of both side axes. The results of the FEA study are given in supplementary information, see Figs. S2 and S3.

Alternatively, and if it is more appropriated for the experiment, a hot air blower can be used instead of the resistive system.

2.2. Synchrotron X-ray experiment

The cell-commissioning synchrotron experiment was carried out using the recently upgraded NCD-SWEET

beamline at ALBA synchrotron (Gonzalez *et al.,* 2018). Powder diffraction data were collected in Debye-Scherrer (transmission) configuration employing a beam with a size of 0.8 mm vertical and 1.2 mm horizontal, and a photon energy of 20 keV (λ = 0.62278 Å) selected with a Si(111) channel-cut crystal monochromator. It was used a Rayonix charge coupled detector LX255-HS (with a pixel size of 44 μm) placed at 313 mm from sample and a tilt vertical angle of 28.92degrees. The active image area was 85×255 mm^2 (h×v). Two dimensional data were collected in 5 different positions along the capillary with an interval of 0.5 mm between them and an exposure time of two seconds per individual pattern.

The cell was rotated at 240 rpm, so the sample did two full rotations per exposure time. The horizontal movement was made with a Micos LS-180 translation stage, part of the beamline equipment and installed just underneath the cell. The raw diffraction data recorded for the empty sapphire capillary (static and under rotation) are displayed in Fig. S4. Fig. S5 shows the calculated positions for the 2D corundum pattern with the Miller indexes. Figs. S4 and S5 show that the diffraction peaks from the cell are well localized on the detector. Therefore, the spots will be masked for the operation and normal azimuthal integration will be performed, see just below. For this commissioning experiment, the diffraction peaks from sapphire were simply removed from the 1D patterns.

The two dimensional data were reduced to 1D data by pyFAI software (Ashiotis *et al.,* 2015). The system was calibrated by using a capillary filled with quartz as standard. The 2D raw diffraction images of this standard, both static and under rotation, are given in Fig. S6.

2.3. Powder diffraction data analysis

Powder patterns were analysed by using the GSAS suite of programs (Von Dreele & Larson, 2004) to obtain Rietveld quantitative phase analyses (RQPA). Final global optimized parameters were: background coefficients, zero-shift error, cell parameters and peak shape parameters using a pseudo-Voigt function (Thompson et al., 1987).

2.4. Oil well cement and paste preparation

A commercial Oil Well Portland cement Class G HSR (Dyckerhoff-Lengerich, Germany), with a Blaine parameter of 340 m^2/kg, was used. Mineralogical composition was determined by RQPA by analysing laboratory X-ray powder pattern collected with Mo-$K\alpha_1$ in a D8 Advance (Bruker) placed at "Servicios Centrales de Apoyo a la investigación (SCAI)" at University of Malaga (Spain) (León-Reina *et al.*, 2016). The laboratory Rietveld fitted pattern is displayed in Fig. S7, with the cement phase analysis reported in the inset.

Cement slurry was prepared by mixing the sample with the corresponding amount of water (water/cement mass ratio equal to 0.47) by hand in a small plastic beaker for 2 min. After that, the paste was immediately loaded into the sapphire capillaries with a syringe and a short piece of silicone tubing. Both ends of the capillaries were blocked with PTFE cylindrical plugs of 2 mm of length and 1.75 mm outside diameter (with tolerance for its width smaller than 0.1 mm).

3. Results and discussion

The spinning cell has been commissioned by measuring the hydration of a commercial oil well cement. These cements are used by the oil industry to support metal oil-well liners and to form a gas tight seal between the bore wall and the liner. The hydration process occurs deep into the ground and it is subjected to elevated pressures and temperatures which depend upon the characteristics of the field application. This cell is intended to reproduce these conditions although the access to higher pressures would be clearly advantageous.

After the calibration study carried out with quartz, see experimental section above, the quality of the diffraction data was assessed with a gypsum sample (powder). A sapphire capillary was filled and powder patterns were collected in static and rotating modes, see Fig. 5. It can be seen that the static pattern presents signatures of texture but because it is a single phase sample, with relatively small particle size, the static pattern yield relatively smooth Debye-Scherrer arches. These data were processed, for the five patterns taken at different positions, as described in the experimental section (first radial integration,

then summation) to yield the one-dimensional powder patterns, see Fig. 6.

The diffraction peak shapes for the gypsum pattern recorded under spinning was slightly better (more symmetric) than those recorded in static conditions. However, it was concluded that the quality of the statically acquired data was good enough for structural studies. The resolution (diffraction peak width) of both data sets is determined by the internal diameter of the used capillary. For the same experimental configuration, narrower capillaries will yield narrower diffraction peaks.

The synchrotron powder patterns of the anhydrous oil well cement at room pressure, static and under spinning, were also recorded for completeness of the experiment. The raw data images are shown in Fig. S8. For the static pattern, it can be seen that many Debye-Scherrer arches are grainy which is due to the large particle size of alite phase (Ca_3SiO_5), the main component of the cement and the low amount of minor phases, which does not ensure random diffracting particles in all directions.

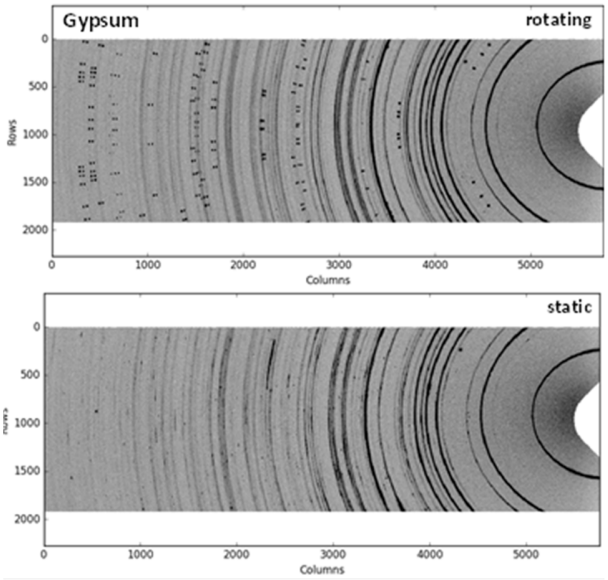

Figure 5
2D synchrotron powder diffraction patterns of the capillary filled with gypsum at room temperature and pressure, (top) rotating and (bottom) static. Diffraction spots from the sapphire are evident in the top pattern and they were masked in the 1D analysis. Note also that sapphire diffraction peaks are split because the two walls of the capillaries are at different distances to the detector.

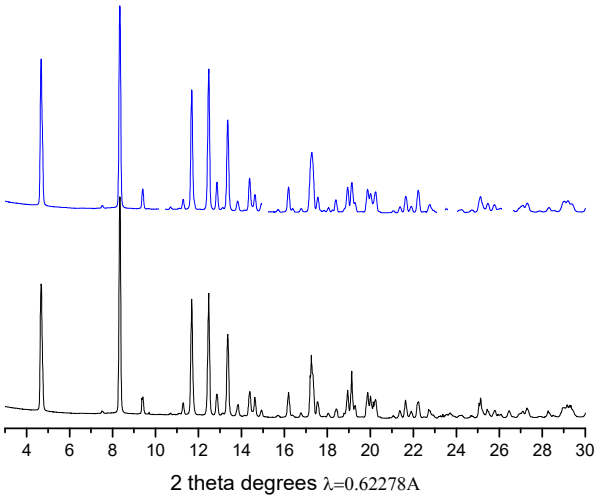

Figure 6
1D synchrotron powder diffraction patterns for gypsum at room temperature and pressure, (top) under rotation and (bottom) static.

The high pressure and high temperature experiment started with the preparation of the cement slurry as described in the experimental section. This slurry was injected into the sapphire tube using a syringe connected with a short piece of silicone tubing. The tubing was then fitted to the capillary assembly taking care to avoid the introduction of air bubbles. Then, two PTFE cylindrical pieces, described in the experimental section, were placed at both side of the slurry to avoid oil contamination along the hydration reaction. These plugs also prevented migration of the slurry to other places in the cell.

After cement slurry loading into the capillary, the cell was closed and oil was pumped into both ends of the system to attain the target pressure. For this experiment, the pressure was set to 150 bars. The measurements were fully consistent in the three pressure evaluation systems, two in the pressure generator and one in the exchange chamber. Once the target pressure was stable a cell-spinning powder pattern was recorded. All the steps, from cement slurry preparation to the collection of the first pattern, took 55 minutes. However, this procedure is under optimisation and the first data set can be recorded in less than 30 min. Then, temperature was increased to 150 ºC. This sequence was chosen because the effect of temperature is larger than that of pressure in cement hydration (Jupe *et al.*, 2011, 2012).

In situ synchrotron X-ray powder diffraction patterns were taken every 15 min. The full experiment lasted 15 hours for studying cement hydration up to a large degree of reaction (in these conditions). The quantitative analysis of all data including the sequences of reactions will be reported elsewhere. Here, we focus on the quantitative analysis of one pattern to highlight the improvement achieved by the use of a spinning cell. The 2D raw data for the cement slurry hydrated for 14 hours (13 h under 150 bars and 150 ºC) are displayed in Fig. 7. This figure compares the patterns collected in static spinning modes. The static pattern is very grainy which lead to poor peak shape of the diffraction peaks and inaccurate intensities after radial integration. This is shown in Fig. 8 where selected diffraction peaks are shown for the five position of the capillary and for the two modes: rotating and static. The smooth rings obtained under rotation, when radially integrated, yield reproducible peak shapes and intensities. Conversely, the grainy rings recorded in the static capillary, when integrated, result in variable peak shapes and intensities. This is partly mitigated when summing up the five 1D patterns, but the resulting powder pattern still presents asymmetric diffraction peak shapes. Larger 2D detectors would improve the particle statistics with 2θ as larger fractions of the Debye-Scherrer rings are collected. For the 2D detector used in this work, the fraction of the recorded reflection changes with the diffracting angle. Therefore, Fig. S9 reports the evolution of selected single peak integrations with 2θ.

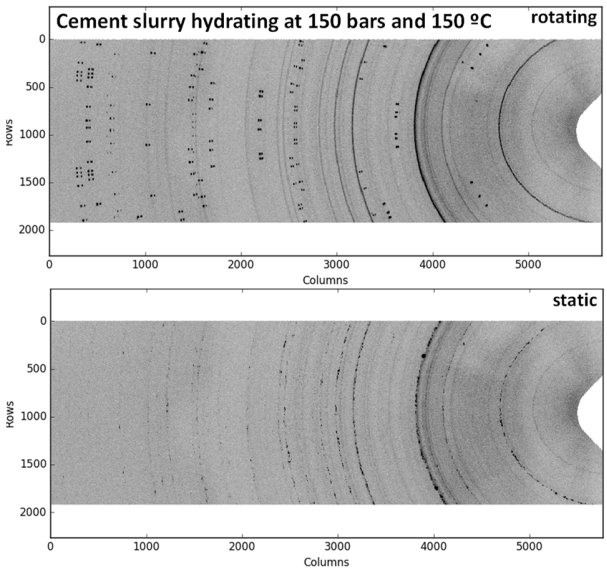

Figure 7

In situ 2D synchrotron powder diffraction patterns of the hydrating cement slurry, 14 h of hydration, at 150 bars and 150 ºC, (top) under rotation and (bottom) static.

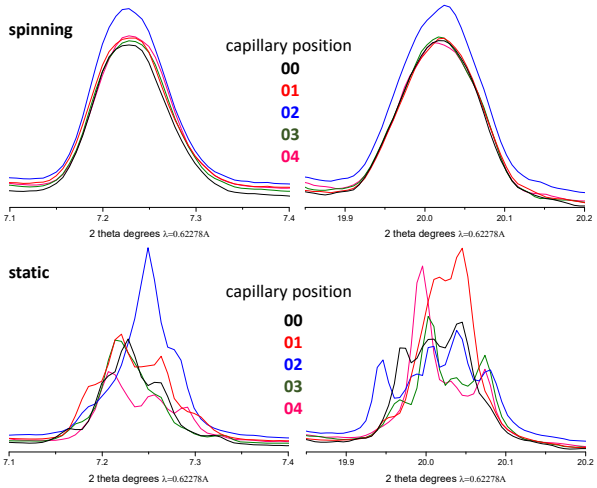

Figure 8
Comparison of the 1D synchrotron powder diffraction peaks at five capillary positions, after radial integration, for hydrating cement slurry at 14 hours, (top) rotating and (bottom) static.

The five powder patterns collected under spinning at 14 hours of hydration where summed with local software, to yield the final data set that was fitted by the Rietveld method. Fig. 9 shows the synchrotron Rietveld plot after the analysis. This fit does not take into account the amorphous phases and the signals from sapphire capillary were masked. The RQPA results are reported in Table 1. It is highlighted that α-$Ca_2SiO_4{\cdot}H_2O$ and Jaffeite phases are only obtained in cement hydration at high pressures (Meller *et al.*, 2007; Palou *et al.*, 2014; Kuzielová *et al.*, 2017).

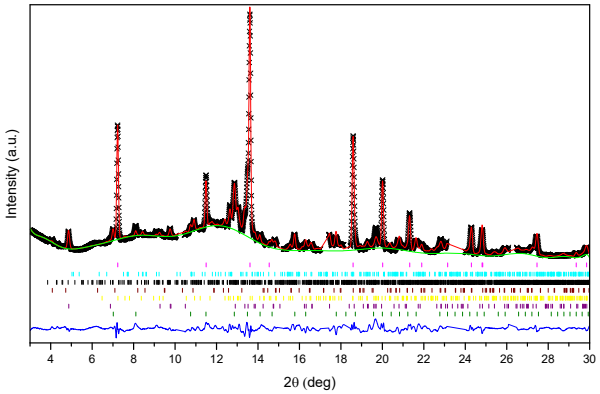

Figure 9

In situ 1D Rietveld synchrotron powder diffraction plot for the oil well cement slurry after 14 h of hydration under 150 bars and 150 ºC.

Table 1. Selected details for the RQPA of the oil well cement slurry after 14 h of hydration under 150 bars and 150 ºC.

Phase	Content (wt%)	R_F (%)	ICSD code
Ca_3SiO_5 – M_3	4.1(3)	14.8	94742
Ca_2SiO_4 – β	15.7(3)	13.4	81096
Ca_2AlFeO_5	22.0(2)	9.1	9197
$Ca(OH)_2$	35.0(1)	3.2	15471
$Ca_2SiO_4{\cdot}H_2O$ – α	5.6(3)	16.1	73404
Katoite	16.7(2)	8.3	49772
Jaffeite	0.8(2)	19.8	39725

The quality of the quantitative phase analysis is judged to be very good based on two observations. Firstly, the difference curve, see bottom blue line in Fig. 9, is quite flat reflecting a good agreement between the measured (crosses) and calculated (red line) patterns. Secondly, and very importantly, the R_F factors are quite low. For a detailed discussion of R-factors in the Rietveld fits, the readers are referred to publications dealing with this topic (McCusker *et al.*, 1999; Toby, 2006). Here, we highlight that R_F factors are phase-dependent and they are low if the chosen structural descriptions are adequate and the powder diffraction data have not systematic errors. As expected, low-content phases displayed larger R_F factors.

4. Conclusions

This new spinning capillary cell has been successfully operated up to 200 bars and 200 ºC. It has been designed to reduce the stress into the capillary imposed by the rotation torque. Furthermore, the improvement in powder diffraction data quality is obvious and it has allowed an *in situ* Rietveld quantitative phase analysis of a hydrating oil well cement at 150 bars and 150 ºC. The cell is now open to users but through collaboration with ALBA staff.

Outlook

The pressure limit of the cell has not been reached so far. Under 200 bars and with a limit speed of 250 rpm no capillary has been broken so far, in all tests. It will be interesting in the future to reach pressures close to 500 bars. Some modifications are needed in order to reach this goal, especially in the rotating PTFE seals and some fittings attached to the side supports. Other possible improvement would be a more compact design which would allow the cell to be implemented in laboratory X-ray powder diffractometers with molybdenum radiation (Leon-Reina *et al.,* 2016). This compact design allows the cell to be used in confined spaces. Furthermore, it would fit within Eulerian cradles present in many synchrotron powder diffractometers. In this case, very high-resolution powder patterns will be collected as the multicrystal analyser setups could be used. This configuration will profit most from the performances of this cell as point detectors will be employed.

Acknowledgements

The design, production and commissioning of this cell was carried out at the ALBA synchrotron as part of Edmundo Fraga's PhD project. This work was financially supported by the Spanish Ministry of Economy and Competitiveness through Grants BIA2014-57658-C2-1-R and BIA2017-82391-R which are co-funded by FEDER. We are grateful to Prof. Angus Wilkinson, Georgia Institute of Technology Atlanta, for sharing his knowledge and details on the high pressure cell developed by his team. We also thank Dr. Marcus Paul, Dyckerhoff-Lengerich, Germany, for fruitful discussion on Oil Well Cements. The cell was commissioned at BL11-NCD-SWEET beamline.

References

Aranda, M. A. G. (2016). *Crystallogr. Rev.* **22**, 150–196.

Ashiotis, G., Deschildre, A., Nawaz, Z., Wright, J. P., Karkoulis, D., Picca, F. E. & Kieffer, J. (2015). *J. Appl. Crystallogr.* **48**, 510–519.

Azhdari, A., Nemat-Nasser, S. & Rome, J. (1998). *Int. J. Fract.* **94**, 251–266.

Chupas, P. J., Chapman, K. W., Kurtz, C., Hanson, J. C., Lee, P. L., Grey, C. P. & IUCr (2008). *J. Appl. Crystallogr.* **41**, 822–824.

Von Dreele, R. B. & Larson, A. C. (2004). *Los Alamos Natl. Lab. Rep. LAUR*. **748**, 86–748.

González, J. B., González, N., Colldelram, C., Ribó, L., Fontserè, A., Jover-Manas, G., Villanueva, J., Llonch, M., Peña, G., Gevorgyan, A., Nikitin, Y., Martínez, J. C., Kamma-Lorger, C., Solano, E., Sics, I., Ferrer, S. & Malfois, M. (2018). *Mechanical Engineering Design of*

Synchrotron Radiation Equipment and Instrumentation (MEDSI), Paris.

Hansen, B. R. S., Møller, K. T., Paskevicius, M., Dippel, A.-C., Walter, P., Webb, C. J., Pistidda, C., Bergemann, N., Dornheim, M., Klassen, T., Jørgensen, J.-E., Jensen, T. R. & IUCr (2015). *J. Appl. Crystallogr.* **48**, 1234–1241.

Ida, T., Goto, T., Hibino, H. & IUCr (2009). *J. Appl. Crystallogr.* **42**, 597–606.

Jensen, T. R., Nielsen, T. K., Filinchuk, Y., Jørgensen, J.-E., Cerenius, Y., Gray M. C., Webb, C. J. (2010). *J. Appl. Crystallogr.* **43,** 1456–1463.

Jupe, A. C. & Wilkinson, A. P. (2006). *Rev. Sci. Instrum.* **77**, 113901.

Jupe, A. C., Wilkinson, A. P. & Funkhouser, G. P. (2011). *J. Am. Ceram. Soc.* **94**, 1591–1597.

Jupe, A. C., Wilkinson, A. P. & Funkhouser, G. P. (2012). *Cem. Concr. Res.* **42**, 1083–1087.

Kuzielová, E., Žemlička, M., Másilko, J. & Palou, M. T. (2017). *Geothermics*. **68**, 86–93.

León-Reina, L., García-Maté, M., Álvarez-Pinazo, G., Santacruz, I., Vallcorba, O., De La Torre, A. G. & Aranda, M. A. G. (2016). *J. Appl. Crystallogr.* **49**, 722–735.

McCusker, L. B., Von Dreele, R. B., Cox, D. E., Louër, D. & Scardi, P. (1999). *J. Appl. Crystallogr.* **32**, 36–50.

Meller, N., Hall, C., Kyritsis, K. & Giriat, G. (2007). *Cem. Concr. Res.* **37**, 823–833.

Palou, M., Živica, V., Ifka, T., Boháč, M. & Zmrzlý, M. (2014). *J. Therm. Anal. Calorim.* **116**, 597–603.

Sakaki, K., Kim, H., Machida, A., Watanuki, T., Katayama, Y., Nakamura, Y. & IUCr (2018). *J. Appl. Crystallogr.* **51**, 796–801.

Thompson, P., Cox, D. E. & Hastings, J. B. (1987). *J. Appl. Crystallogr.* **20**, 79–83.

Toby, B. H. (2006). *Powder Diffr.* **21**, 67–70.

van Beek, W. & Pattison, P. (2018) Capillary cells. In International Tables for Crystallography. Vol. H – Powder Diffraction. Edited by Gilmore, C. J., Kaduk, J. A. & Schenk, H. Chapter 2.9, 189-192.

Revised Supporting Information for

High pressure and temperature spinning capillary cell for *in situ* synchrotron X-ray powder diffraction

Edmundo Fraga,[a,b] Armando Yáñez,[b] Jesus D. Zea-Garcia,[c] Angeles G. De la Torre,[c] Ana Cuesta,[c] Ricardo Valcárcel-Fernández,[a] Francesc Farré-París,[a] Marc Malfois,[a] Miguel A. G. Aranda[a,*]

[a]ALBA Synchrotron, Carrer de la Lum, 2-26, 08290 Cerdanyola del Vallès, Barcelona, Spain. [b]Universidade da Coruña, Dpto. Departamento de Ingeniería Naval e Industrial, Campus de Esteiro s/n, 15403 Ferrol, A Coruña, Spain. [c]Departamento de Química Inorgánica, Universidad de Málaga, Campus Teatinos S/N, 29071 Málaga, Spain *Correspondence e-mail: migarcia@cells.es

This document contains nine figures.

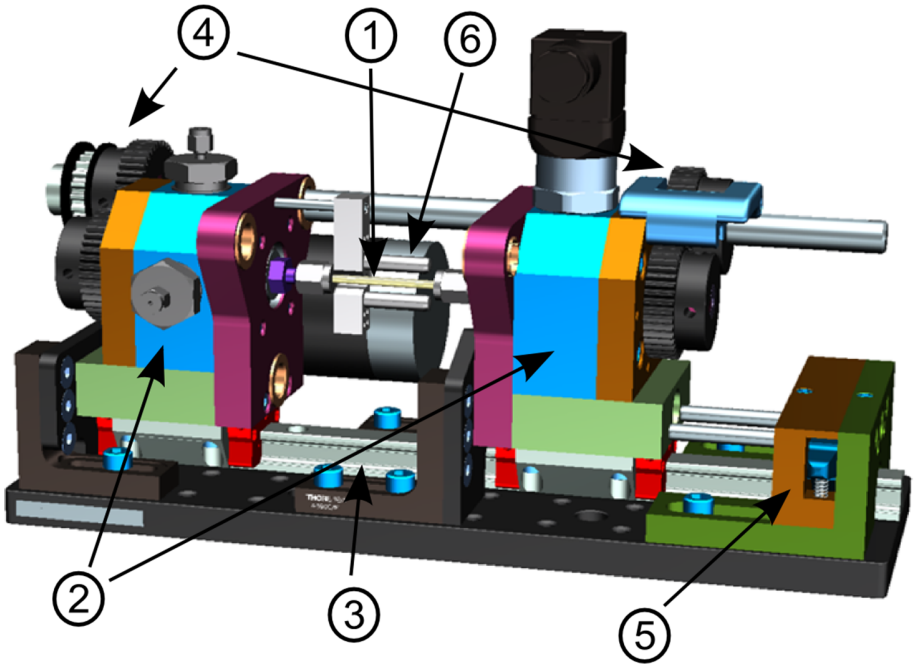

Figure S1. General description of the main components of the spinning cell over the 3D design. Main components: 1. Sample holder (removable capillary). 2. Side supports. 3. Linear displacement system. 4. Transmission system. 5. Spring lock system. 6. Heating system.

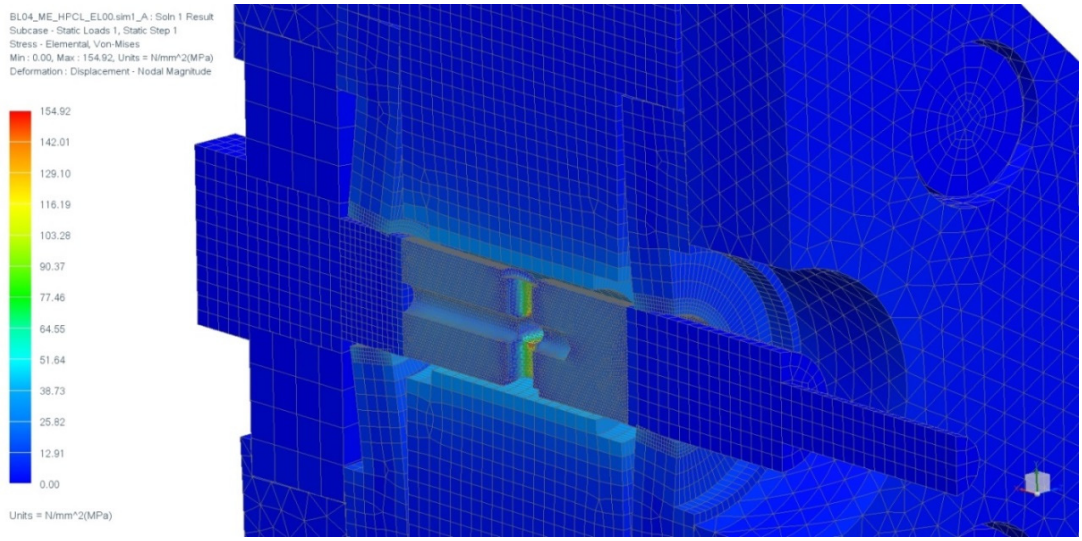

Figure S2. Equivalent tensile stress results from the Finite Element Analysis. All the stresses are below the yield strength limit. The highest stresses are very localized and coincident with the sharp edges on the entrance to the main axis, being the rest of the locations negligible when compared to the yield strength limit.

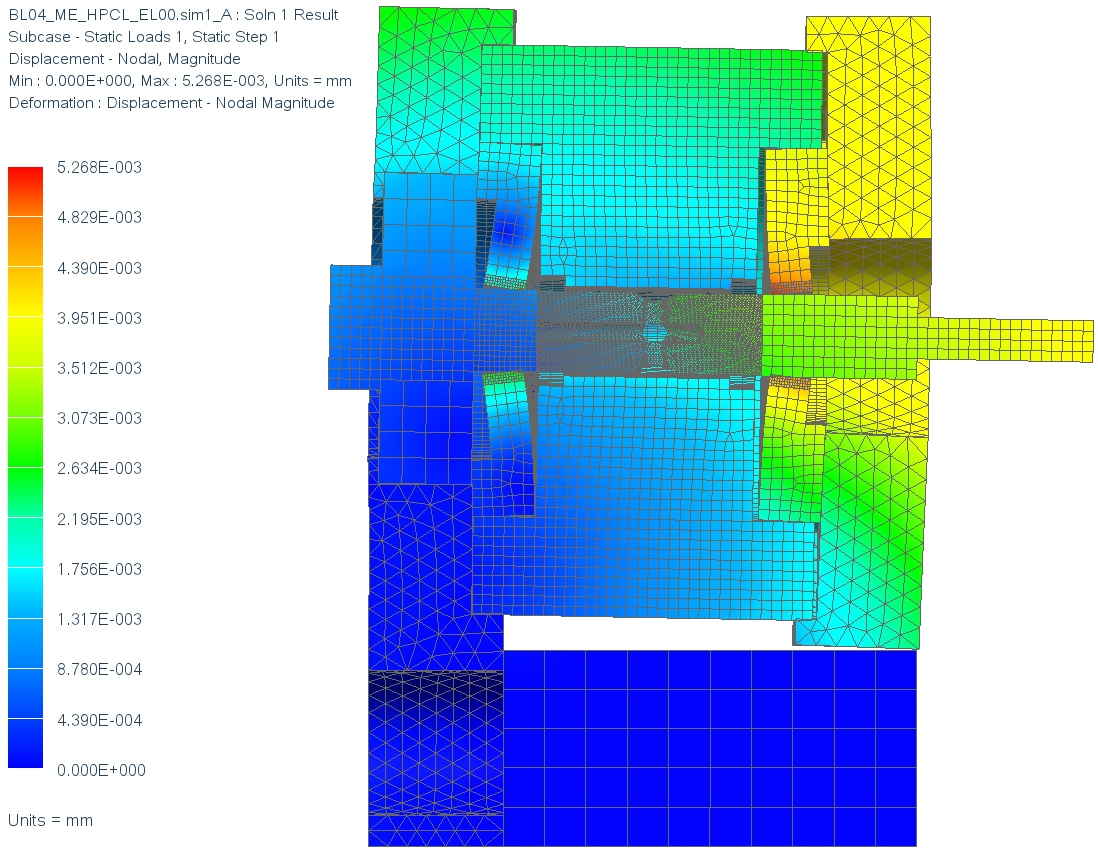

Figure S3. Nodal displacement results from the Finite Element Analysis. The pressure applied inside the exchange chamber is 20 MPa (200 bars) and the image has a deformation scale factor of 200 % of the absolute value in order to visualize the deformed mesh.

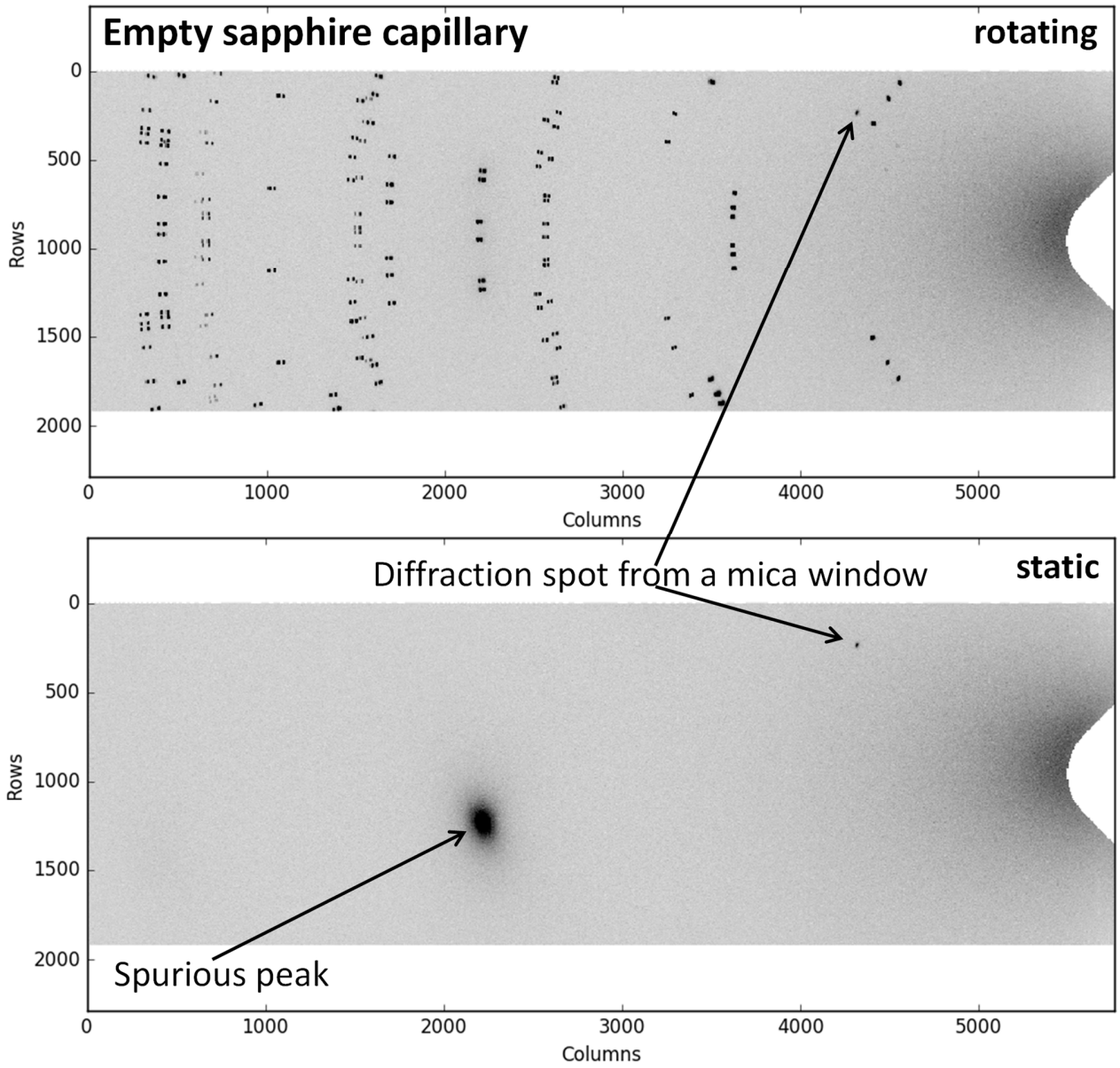

Figure S4. 2D powder diffraction patterns of the empty sapphire capillary, (top) rotating and (bottom) static. Diffraction spots from the sapphire are evident in the top pattern, at the expected position from its crystal structure. It can also be noted that sapphire diffraction peaks are split because the two walls of the capillaries are at different distances to the detector.

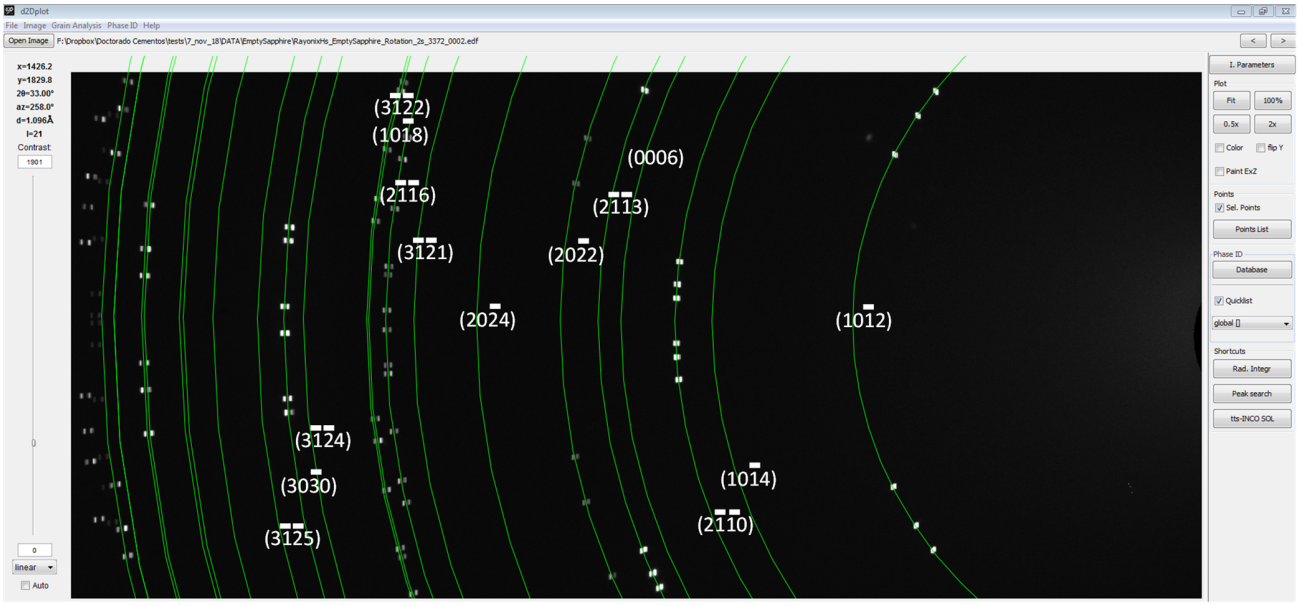

Figure S5. 2D powder diffraction patterns of the empty sapphire capillary (white spots) with the calculated corundum powder pattern (green lines) listing the Miller indexes.

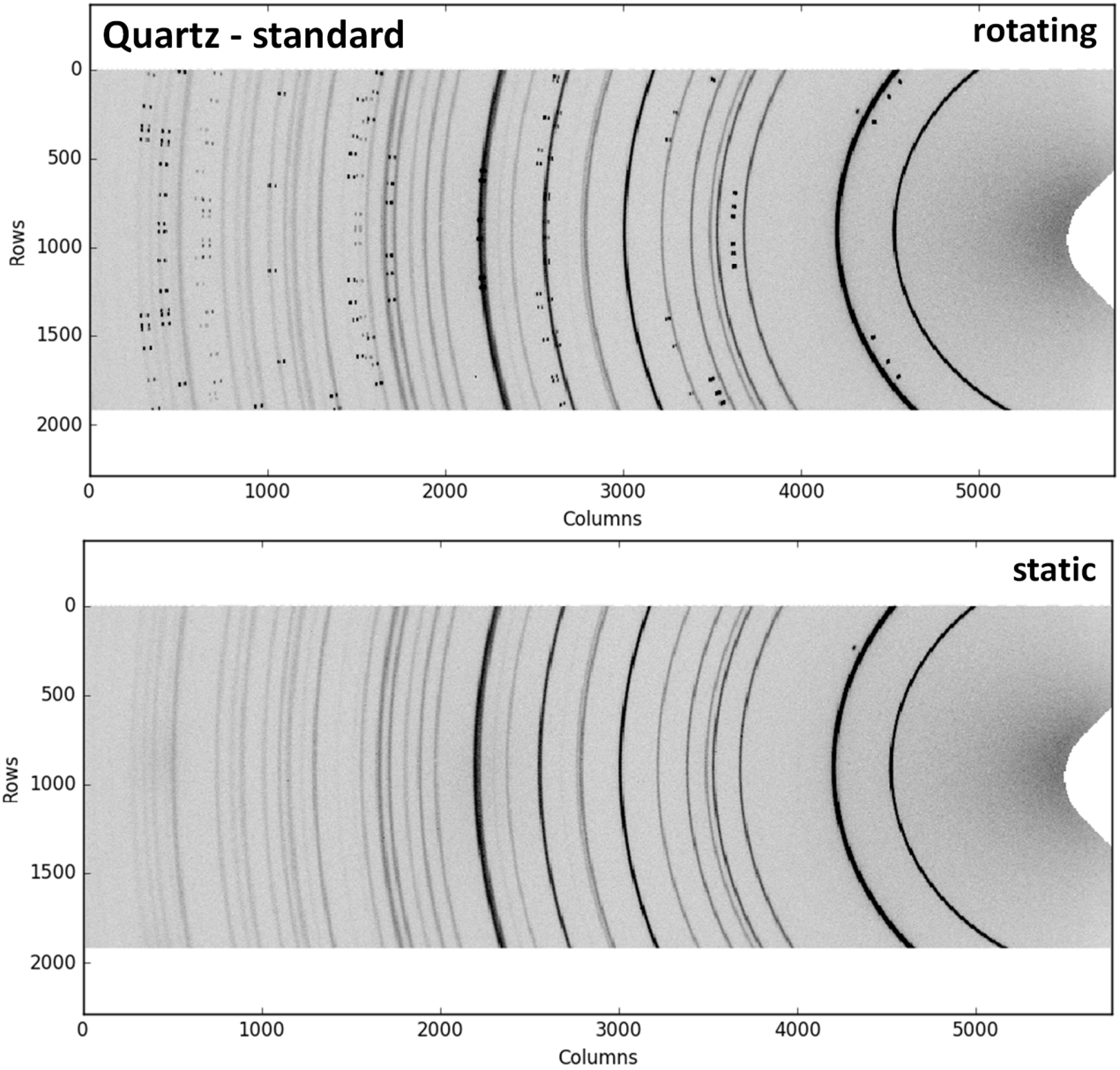

Figure S6. 2D powder diffraction patterns of the capillary filled with quartz used as standard at room temperature and pressure, (top) rotating and (bottom) static.

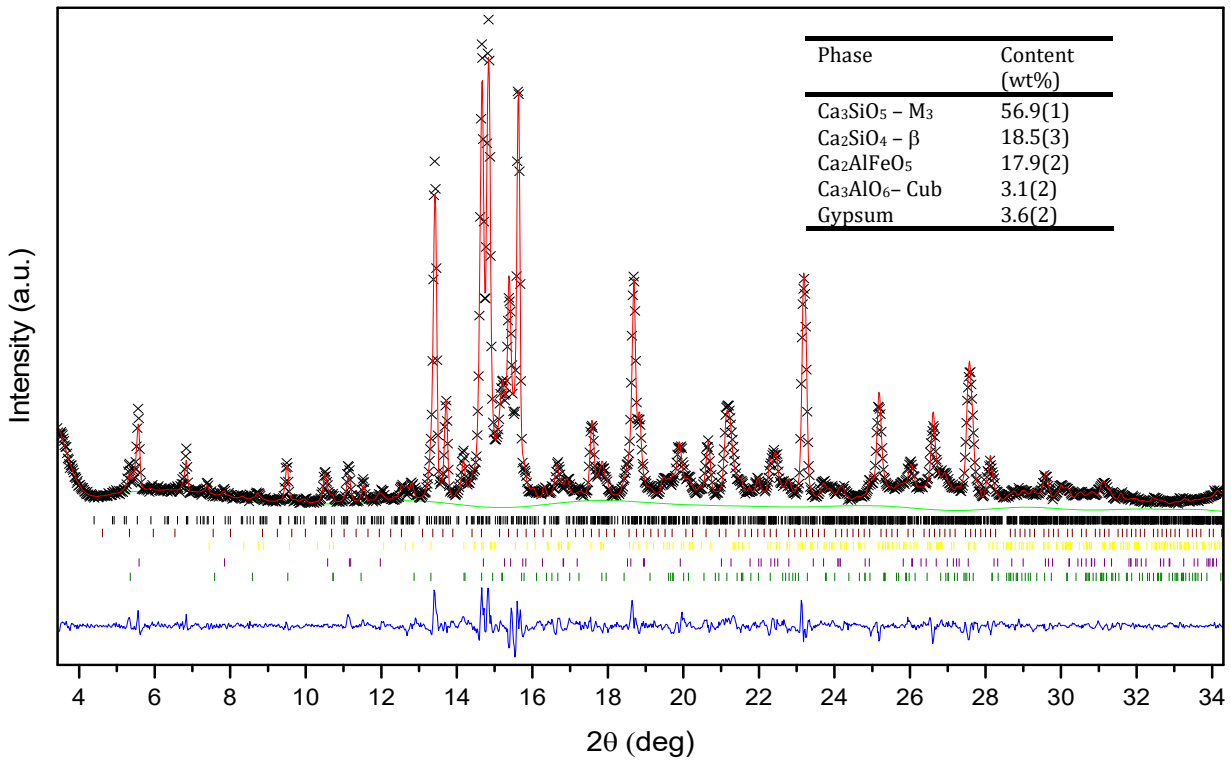

Figure S7. Rietveld plot for the laboratory X-ray powder diffraction pattern of the as-received oil well cement (Mo $K\alpha_1$ radiation). Rietveld quantitative phase analysis results are given in the inset.

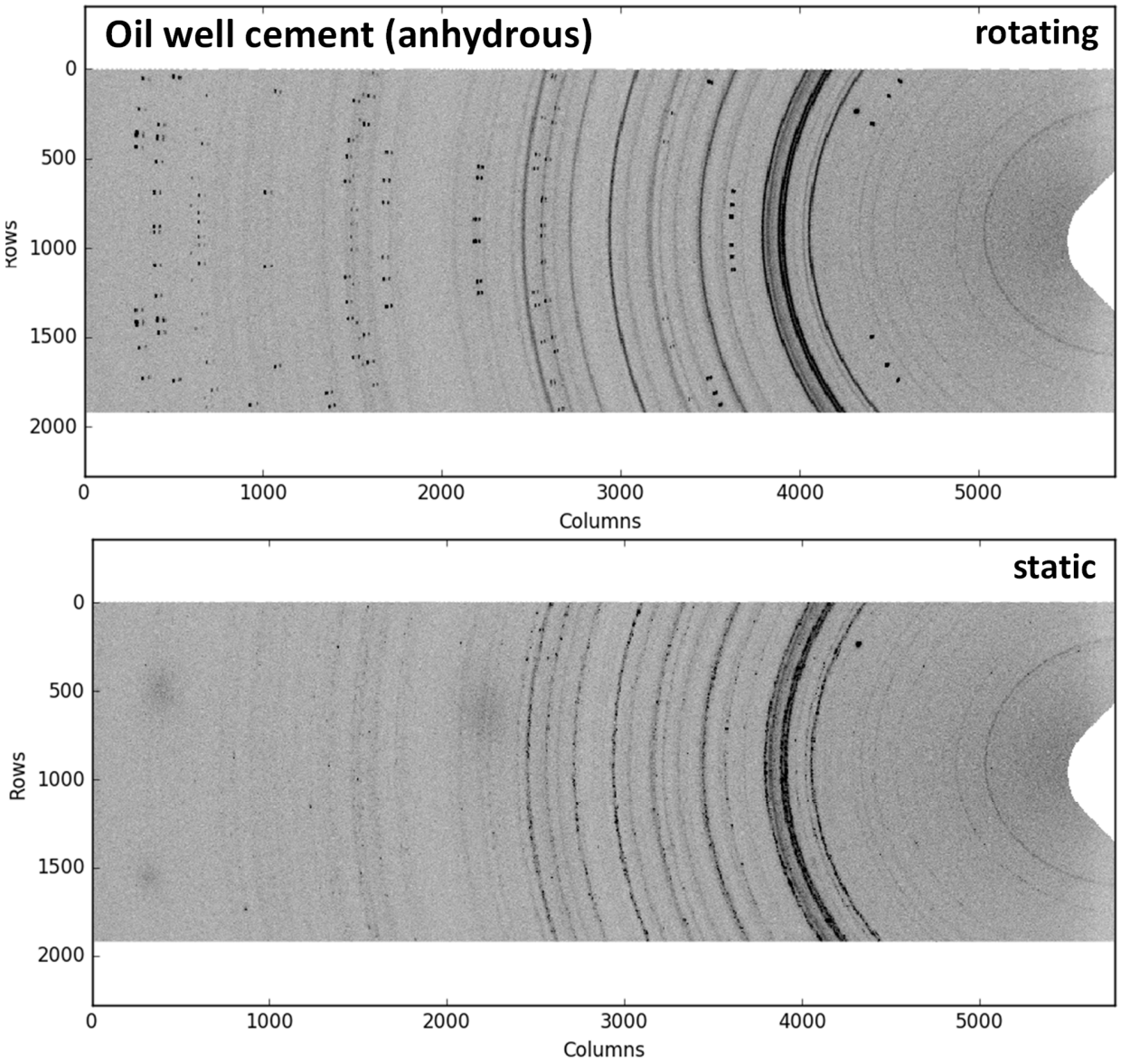

Figure S8. 2D powder diffraction patterns of the oil well cement (anhydrous) at room temperature and pressure, (top) rotating and (bottom) static.

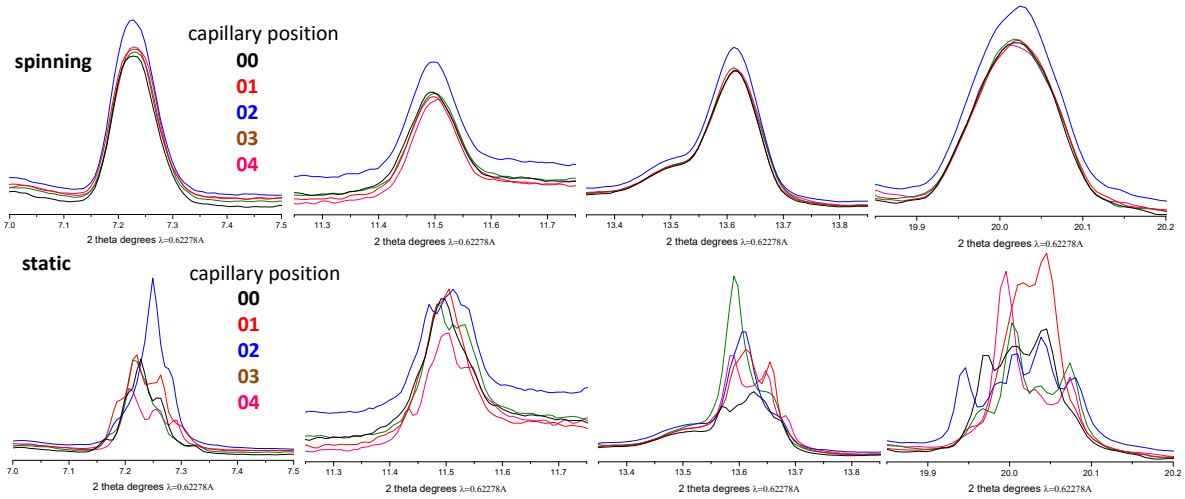

Figure S9. Comparison of the 1D synchrotron powder diffraction peaks at five capillary positions, after radial integration, for hydrating cement slurry at 14 hours, (top) rotating and (bottom) static. The evolution with 2θ is highlighted for four selected regions.